ADVANCED FUNCTIONAL MATERIALS
www.afm-journal.de

3D Micro-Extrusion of Graphene-based Active Electrodes: Towards High-Rate AC Line Filtering Performance Electrochemical Capacitors

Teressa Nathan-Walleser, Ion-Matei Lazar, Martin Fabritius, Folke Johannes Tölle, Qi Xia, Bernd Bruchmann, Shyam S. Venkataraman, Matthias Georg Schwab, and Rolf Mülhaupt**

A facile one-step printing process by 3D micro-extrusion affording binder-free thermally reduced graphene oxide (TRGO) based electrochemical capacitors (ECs) that display high-rate performance is presented. Key intermediates are binder-free TRGO dispersion printing inks with concentrations up to 15 g L^{-1}. This versatile printing technique enables easy fabrication of EC electrodes, useful in both aqueous and non-aqueous electrolyte systems. The as-prepared TRGO material with high specific surface area (SSA) of 593 m^2 g^{-1} and good electrical conductivity of ≈16 S cm^{-1} exhibits impressive charge storage performances. At 100 and 120 Hz, ECs fabricated with TRGO show time constants of 2.5 ms and 2.3 ms respectively. Very high capacitance values are derived at both frequencies ranging from 3.55 mF cm^{-2} to 1.76 mF cm^{-2}. Additionally, these TRGO electrodes can be charged and discharged at very high voltage scan rates up to 15 V s^{-1} yielding 4 F cm^{-3} with 50% capacitance retention. Electrochemical performance of TRGO electrodes in electrolyte containing tetraethyl ammonium tetrafluoroborate and acetonitrile (TEABF4-ACN) yields high energy density of 4.43 mWh cm^{-3} and power density up to 42.74 kW cm^{-3}, which is very promising for AC line filtering application and could potentially substitute state of the art electrolytic capacitor technology.

1. Introduction

Electrolytic capacitors are used in large quantities in electric circuits where high currents or low frequencies are involved. One of the most common applications of electrolytic capacitor is in power supply circuits as decoupling capacitors where they are used to suppress high-frequency noise in power supply signals.[1] They are very cost effective and able to provide a larger capacitance per volume than other types of conventional electrostatic capacitors.[2] However, they have limited frequency response as their equivalent series resistance (ESR) increases with frequency, thus restricting their use to frequencies below 100 kHz. Electrolytic capacitors also encounter major hurdles when it comes to applications that require small scale device design. Miniaturization of electrolytic capacitors is challenging as there are many parameters to be considered such as the geometric area of electrodes, dielectric property of the oxide layer, and electrolyte, and so forth.[1–3] Hence, new solutions for efficient energy storage technologies along with continuous miniaturization are required in order to address these challenges.

Electrochemical capacitors (ECs) are unique energy storage devices with complementary properties to Li-ion batteries, and are often considered as promising candidates for alternative energy storage as a result of their pulse power supply, long cycle life, and low maintenance cost.[4–6] Utilization of ECs in applications such as on-chip energy storage[7–10] and ac-line filtering[11–13] is made possible with the current advancement in electronics fabrication technology. The time constant of ECs is significantly higher than that of electrolytic capacitors because of the nature of the electrode active material. In ECs activated carbon is dominantly used as electrode material, which is largely mesoporous in nature, and therefore limits the rapid signal propagation. At 120 Hz, EC devices containing activated carbon electrodes function more like resistors than capacitors which makes them incompatible for ac-line filtering.[11] Other forms of carbon such as conductive carbon black and graphene have been recently demonstrated as potential materials for ac-line filtering application. Kossyrev et al. demonstrated a RC time constant of 354 µs at 120 Hz using a special grade conductive carbon black as an alternative active material.[12] Inkjet printing of this active material directly on the separator membrane of the device yielded a capacitance of 800 µF.[11] Miller et al. has demonstrated that

Dr. T. Nathan-Walleser, Dr. S. S. Venkataraman, Dr. M. G. Schwab
Carbon Materials Innovation Center (CMIC), BASF SE
67056 Ludwigshafen, Germany
E-mail: matthias.schwab@basf.com
I.-M. Lazar, M. Fabritius, F. J. Tölle, Prof. R. Mülhaupt
Freiburg Materials Research Center (FMF)
and Institute of Macromolecular Chemistry University of Freiburg
Stefan-Meier-Str. 31, D-79104 Freiburg, Germany
E-mail: rolf.muelhaupt@makro.uni-freiburg.de
Dr. Q. Xia, Dr. B. Bruchmann
Joint Research Network on Advanced Materials and Systems (JONAS), BASF SE
67056 Ludwigshafen, Germany

DOI: 10.1002/adfm.201304151

vertically oriented graphene sheet based ECs yield RC time constant of less than 200 μs at 120 Hz frequency.[11] The superior performance is attributed to the direct growth of graphene with special geometry and edge conformation on the metal current collectors by high temperature chemical-vapor deposition (CVD) method.[11] However, the electrode preparation and fabrication technique might not be cost effective for large scale production. Sheng et al. has attempted an alternative method to prepare electrodes using electrochemically reduced graphene oxide. By this method, RC time constant of 1.35 ms at 120 Hz was achieved with specific capacitance of 283 μF cm^{-2} and high scan rate ability up to 350 V s^{-1} were reported. [13]

In this work, we report the electrochemical performance of thermally reduced graphene oxide (TRGO) with an objective to demonstrate the suitability of a scalable and dispersible binder-free highly concentrated TRGO ink using a novel approach which was published in our earlier work.[14] Conventionally, the direct printing of electrically conductive graphene inks using techniques such as inkjet printing or screen printing has been demonstrated as a practical and low-cost method for the fabrication of EC electrodes.[15–18] However, in particular inks used in inkjet printing have high requirements regarding their particles sizes, viscosity and surface tension which must be carefully aligned to the printing process.[16,19] Importantly, only graphene dispersions of rather low concentrations (up to 2 g L^{-1})[17,20–22] can be used for formulating inks. The stable dispersion of graphene in these inks is another important prerequisite for the development of solvent-based large-scale graphene processing for applications in energy storage devices.[23,24] Graphene dispersions usually show a steep increase in viscosity as a function of the graphene content resulting in the mandatory use of surfactants for aqueous systems[17,20,21] or toxic, high boiling point solvents when organic media are chosen (such as *N*-methyl pyrrolidone or dimethyl formamide).[25,26] In general, these aspects are unfavorable for integrating electrodes derived from such inks in EC devices. Surfactants and other additives will necessarily be embedded into the final electrode assembly or leach into the electrolyte and thereby may disturb the proper electrical function of the EC. Hazardous solvents are poorly compatible to the preferred processing protocols of industry that are defined by an increasing demand for green chemistry. Frequently, their high boiling points add further complexity and energy consumption to the drying step of the electrodes.

In this work, we employ high pressure homogenization (HPH) which is facile and very easy to use for the fabrication of printable TRGO inks in large quantities with the use of common and environmental benign solvents, such as water, ethanol or *iso*-propanol. Dispensing of the resulting concentrated binder-free TRGO dispersions is achieved by means of 3D micro-extrusion. In contrast to inkjet printing, 3D micro-extrusion is extraordinary in 3D printing with respect to both its tolerance of high viscosity and broad choice of materials ranging from metal and ceramic pastes to polymer melts, dispersions and even three-dimensional hydrogel scaffolds for tissue engineering.[27,28] It is equipped with a computer-guided 3D positioning of a printing head, as seen with CNC milling machines. The printing head contains a nozzle which is similar to a syringe equipped with changeable needle tips. To release the ink pneumatic pressure is used, which can be tuned continuously. Neither mechanical valves nor piezoelectric or ultrasonic dispensing are required. By adjusting the pressure and the nozzle's inner diameter according to the given viscosity parameters, the processing of dispersions with viscosities up to 1000 Pa s is possible.[14] 3D objects with thicknesses up to 3 cm can be fabricated precisely and rapidly on an area up to 10 cm × 14 cm.[14] For instance, conductive paths with reasonably good resolutions of about 250 μm and film-thickness of about 5 μm were fabricated with a single printing step.[14]

Following a "top-down" strategy using natural graphite as a starting material, thermal reduced graphene oxide (TRGO), was prepared at large scale and from low cost feedstock materials.[29–32] Binder and surfactant-free TRGO-based electrodes were then prepared from stable and highly concentrated TRGO inks using the 3D micro-extrusion method as discussed above and as shown in **Figure 1**. Compared to methods like the doctor blade, the number of layers and their thickness are easier to adjust with 3D micro-extrusion. Additionally, the amount of released ink can be fully controlled, which enables precise and rapid patterning of TRGO dispersions on carbon fabric substrates that serve as current collectors. In sharp contrast to the doctor blade process, several dispensers can be combined, thus enabling simultaneous 3D dispensing of different materials and printing of complex multifunctional structures. Furthermore, unlike metal substrates the use of chemically robust carbon fabrics allows for flexible EC fabrication with aqueous (acid/base), non-aqueous and ionic liquid electrolytes with a wide range of operating potential window. In this work, ECs were fabricated using printed TRGO electrodes and were tested in both aqueous and non-aqueous electrolyte, 1 M KOH and 1 M $TEABF_4$-ACN, respectively. For the purpose of comparison, EC electrodes with a standard activated carbon (DARCO KB-G from Norit) reference material were prepared and studied under identical experimental conditions.

The process scheme in Figure 1 describes the initial preparation of TRGO by thermal exfoliation and reduction of purified graphene oxide (GO). TRGO/iso-propanol dispersions of high viscosity and concentrations were prepared by a high pressure homogenization treatment. Owing to the presence of functional groups on the graphene sheets, neither binders nor surfactant addition is needed to produce concentrated TRGO dispersions.[14,33,34] The oxygen content of TRGO is readily controlled by the reduction temperature.

2. Results and Discussion

2.1. Highly Concentrated TRGO Dispersions Containing Single and Few Layered TRGO Sheets

TRGO materials were prepared by thermal reduction and exfoliation of purified GO in a tube furnace at 400 °C (described in detail in the Experimental Section), following a procedure published elsewhere.[29,30] The essential characterization results measured from the pristine GO and TRGO products are summarized in **Table 1**.

At high temperature, thermal decomposition of the functional groups on GO takes place, leading to a rapid generation of gaseous pressure in between the graphene sheets.[30] During

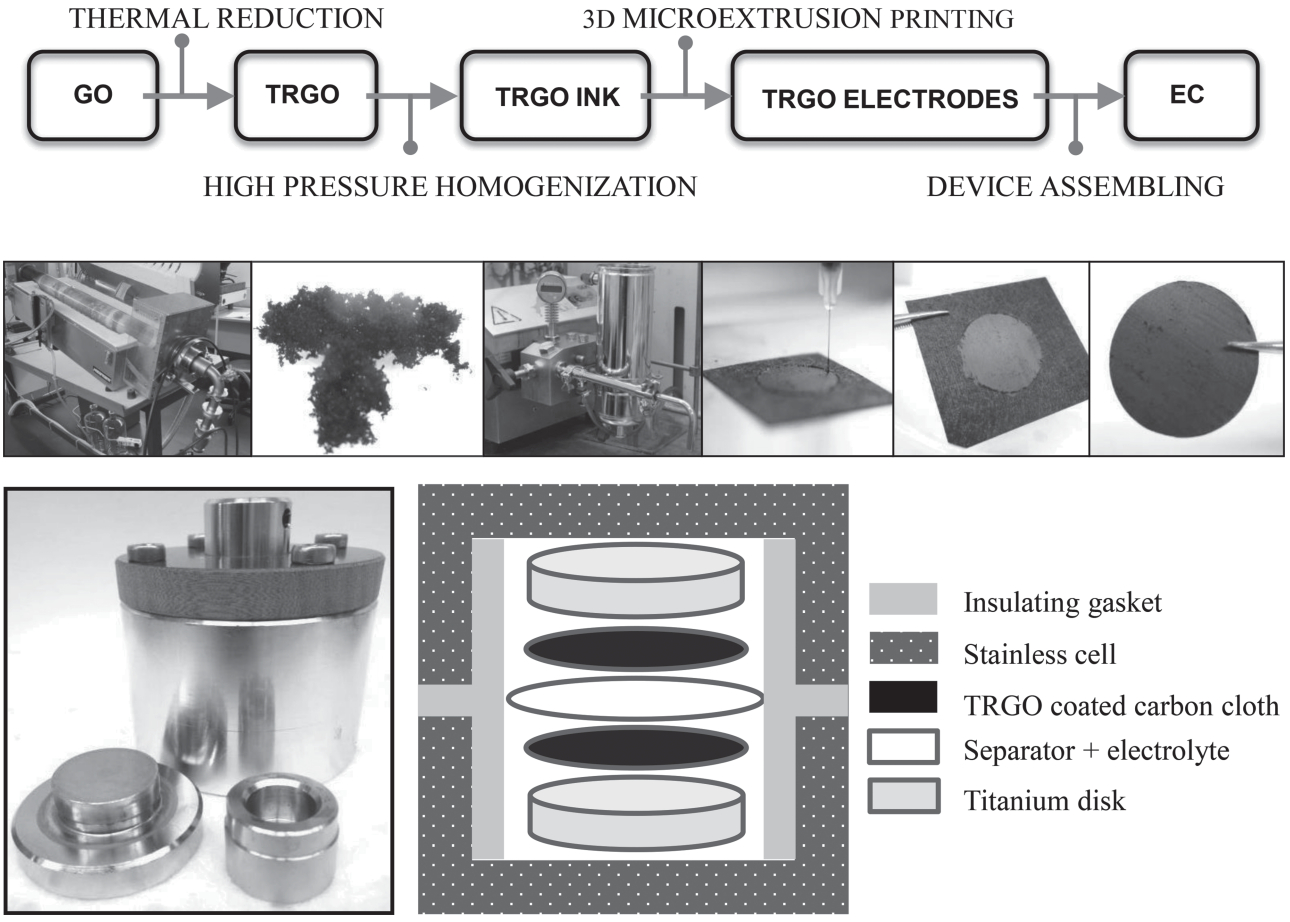

Figure 1. Preparation of high performance EC based on binder-free functionalized graphene electrodes. From top left to top right: Graphite oxide is thermally reduced at 400 °C in a tube furnace; The obtained TRGO is then processed via HPH to form a stable TRGO-iso-propanol dispersion; The ink is printed on carbon cloth using 3D-microextrusion; The electrode is punched out for EC assembling; Image on the bottom: scheme of EC assembly using TRGO printed carbon cloth.

this process, the stacked GO structure is significantly expanded into highly wrinkled sheets, as illustrated by the AFM image in **Figure 2**a. The thickness of the sheets can be as low as 2.3 nm indicated by the line profile analysis in Figure 2b which revealed that the obtained TRGO is mainly composed of less than three stacks of individual graphene sheets. The typical lateral size of the flakes is found to be on the µm scale. This finding is further supported by TEM images in **Figure 3**a,b.

The Brunauer-Emmett-Teller (BET) specific surface area obtained by the dynamic flow gas adsorption technique for afore mentioned TRGO material is 593 m^2 g^{-1}. From Figure 3c, an adsorption isotherm of type IV or isotherms being combination of type IV and type II can be observed. Type II isotherm is the normal form obtained for a non-porous or macroporous material where it represents unrestricted monolayer-multilayer adsorption. The beginning of the almost linear middle section of the isotherm is often taken to indicate the stage at which monolayer coverage is complete and multilayer adsorption is about to begin. Type IV is a variation of type II where the graph at the lower pressure region is quite similar to Type II. This is explained by the formation of a monolayer followed by multilayers. However, at higher pressure, instead of on the open surface, adsorption takes place in the mesopores. The pronounced hysteresis loops (H3) is commonly associated

Table 1. Characterization results measured from TRGO material reduced from purified GO at 400 °C.

Properties	Specific surface area [m^2 g^{-1}]	Conductivity [S cm^{-1}][a)]	Raman spectroscopy			C/O ratio
			D-Band shift [cm^{-1}]	G-Band shift [cm^{-1}]	I_D/I_G	
GO	–	≈10^{-3}	1352	1593	0.95	1.5
TRGO	593[b)]	16	1344	1593	0.84	5.8

[a)]Measured from filtered graphene paper using 4-point measurement; [b)]measured by BET method.

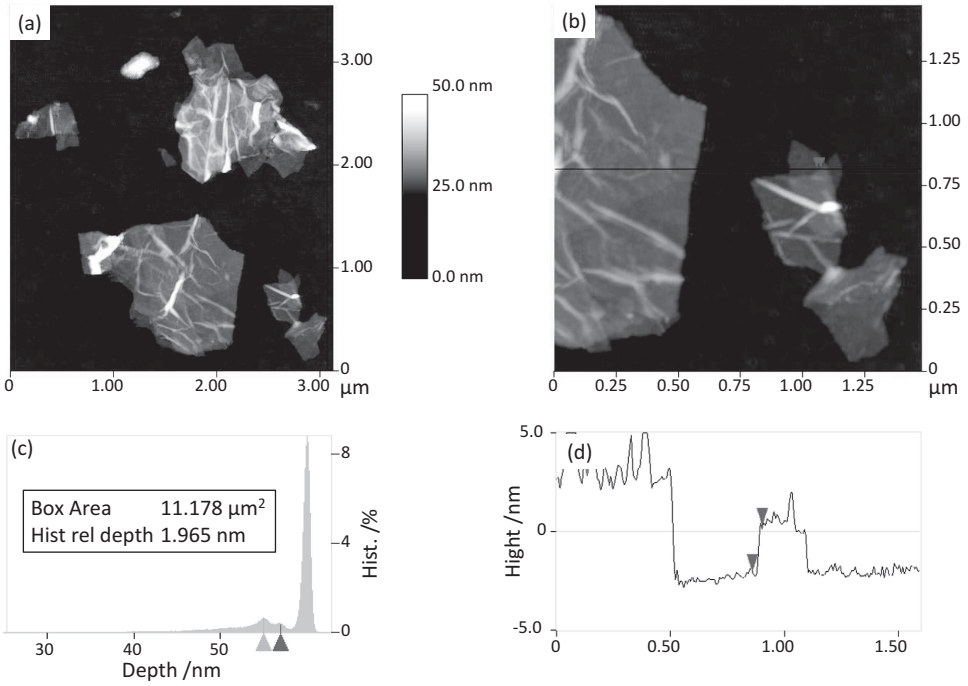

Figure 2. a,c) AFM statistical depth analysis measured from a representative TRGO sheets deposited from briefly exfoliated TRGO dispersion by bath sonication. b,d) AFM section analysis measured from a representative TRGO sheet to show the thickness of one TRGO-sheet.

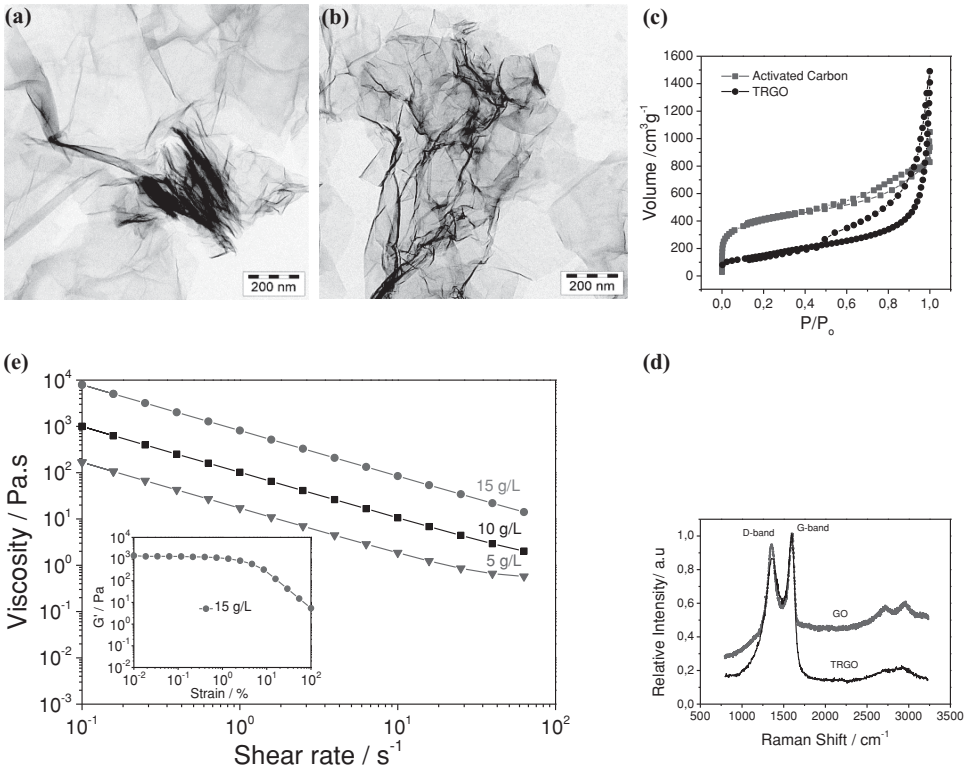

Figure 3. a,b) High-resolution transmission electron microscopy (TEM) image of TRGO. c) Comparison of nitrogen sorption isotherms of activated carbon and TRGO. d) Comparison of Raman spectra measured from TRGO and GO. e) Complex viscosity as a function of the shear rate for TRGO-isopropanol dispersions with different concentrations; (INSET) Storage modulus as a function of the strain from a TRGO-isopropanol dispersion with a concentration of 15 g L^{-1}.

with capillary condensation within mesopores.[35,36] It does not exhibit any limiting adsorption at high $P/P_{o,}$ and it is observed in materials that have aggregates of plate-like particles giving rise to slit-shaped pores.[36]

Type H3 loop suggest that the TRGO material indicates non-rigid aggregates of plate-like particles or slit-shaped pores.[36] Closure at $P/P_o \approx 0.4$ indicates the presence of small mesopores. An isotherm of the activated carbon which was used as electrode material for comparison purpose was also recorded. It shows H4 hysteresis loop which are generally observed for materials containing both microporous and mesoporous structures. The BET specific surface area obtained for this activated carbon is ≈1400 $m^2 g^{-1}$. The presence of open pores structure in TRGO can be seen as the vertical tails of adsorption branches at the $P/P_o \approx 1.0$, showing no distinctive plateau.[36] Large nitrogen adsorption uptakes at $P/P_o > 0.9$ is a typical characteristic of nanostructured materials as adsorption for high relative pressures occurs for materials that are of high surface-to-volume ratio. This allows better accessibility for the ionic charges within the 3D conductive network which increases charge storage capability.[37,38]

Figure 3d compares the Raman spectra measured from GO and TRGO reduced at 400 °C. The results showed the usual D and G peaks for GO around 1352 and 1593 cm^{-1}. The broad and intensive D-band at 1352 cm^{-1} is associated with the disrupted sp^2 domains by the oxygen-containing functionalities in-planes and on-edges indicating higher degree of structural disorder which can be edges, charge puddles, ripples, or any other defects.[39,40] This can be measured using the I_D/I_G peak ratio which is 0.95. A slight decrease of intensity in the D-band for TRGO can be observed. I_D/I_G peak ratio has decreased to 0.84, which attributes to the removal of functional groups and indicates less disordered structure. However, as evidenced by the previously discussed AFM and TEM results, the reduced sheets contain a large number of wrinkles, which account for the significant D-band contribution in the thermally reduced material.

In many applications such as photovoltaic cells, capacitors and transparent electrodes,[41–43] TRGO is more attractive than other graphene materials due to the fact that the surface functionalities and C/O ratio can be conveniently tuned simply by varying the reduction temperature.[14] The presence of oxygenated functional groups on TRGO facilitates easier dispersion in isopropanol without any further formulation of the inks containing dispersants or surfactants. In the final ECs devices, the remaining oxygenated functional groups improve the wettability of the electrodes in electrolyte solution.[44] A clear hump in the CV can be observed during the first few cycles, which suggests the occurrence of redox reactions. However this process is irreversible and diminished in the subsequent cycles.[45]

TRGO dispersions prepared via HPH method typically contain single to few layered graphene sheets and are stable in various types of polar solvents at high concentration.[14] The HPH uses high pressure to push the dispersion out though a narrow gap, where resulting sheer forces then exfoliate the TRGO stacks. In comparison to other high energetic exfoliation techniques, such as horn sonication, ball milling, high speed mixing, the HPH method represents a continuous process of high output of about 10 L h^{-1},[14] determined by the scale of the high-pressure-homogenizer used.

Furthermore, inks with high graphene content are available by this procedure with concentrations of up to 15 g L^{-1}. Compared to inkjet printing, where the concentration is limited to ≈ 2.0 g L^{-1} in aqueous[17,20–22] and ≈ 0.12 g L^{-1} in organic solvents[46,47] and an overall low viscosity < 0.1 Pa s is required,[48,49] the high TRGO content processable by 3D micro-extrusion enables a fast production and the potential for the avoidance of the time-consuming repetition of multiple printing steps.[14] In this work, TRGO/iso-propanol dispersions were processed with HPH treatments using homogenization pressures of as high as 1000 bar. The dispersions can be readily used for printing and no pre and post-treatments, such as centrifugation, filtration, or further reduction, are necessary. The viscosity shows an exponential trend with increasing TRGO content (Figure 3e). At a scan rate of 1 s^{-1} the complex viscosity of the used ink with 1.5 wt% TRGO is 815 Pa s and shows a plateau modulus at 10^3 Pa, which enables good form stability of the desired shape while plotting, but enough mobility to form a continuous film during the drying process.

2.2. Fabrication of the TRGO-based Active Electrodes by the 3D Micro-Extrusion Method

An electrically conductive carbon fabric was used as printing substrate during the 3D micro-extrusion step due to its high corrosion resistance against acid and alkaline electrolytes which makes it very versatile for EC fabrication of all types. The surface conductivity provided by TRGO electrodes printed on an electrically insulating paper was determined by four point probe measurements to be 16 S cm^{-1}. The surface conductivity provided by TRGO electrodes printed on an electrically insulating paper determined by four point probe measurements is ≈ 16 S cm^{-1}. This is one order of magnitude higher than the published results for chemically reduced GO,[42,50,51] which was found to be less than 1 S cm^{-1} and is of comparable order of magnitude to values found for laser scribed GO.[9] FE-SEM image in **Figure 4**a displays the coated and the uncoated area of the carbon cloth, while Figure 4b–d are the cross-sectional observations of the TRGO/flexible carbon fabric electrode that shows the randomly orientated TRGO sheets organized into a highly porous network on top of the support material. The highly wrinkled morphology of the randomly layered TRGO sheets can be clearly observed in between the carbon cloth fibers (Figure 4d) and corroborates with the AFM study of individual flakes (Figure 2).

2.3. Electrochemical Testing of the TRGO-based SCs

The EC devices were fabricated according to the schematic configuration shown in Figure 1 (assembling steps are described in Experimental Section). In each device, two electrodes are impregnated either with aqueous or non-aqueous electrolytes with a separator inserted in between and finally packed in between the titanium encapsulations. **Figure 5**a and b depict the cyclic voltammetry (CV) curves of EC in 1 M KOH and 1 M $TEABF_4$-ACN, respectively, at both high and low voltage scan rates. ECs assembled using TRGO electrodes in both

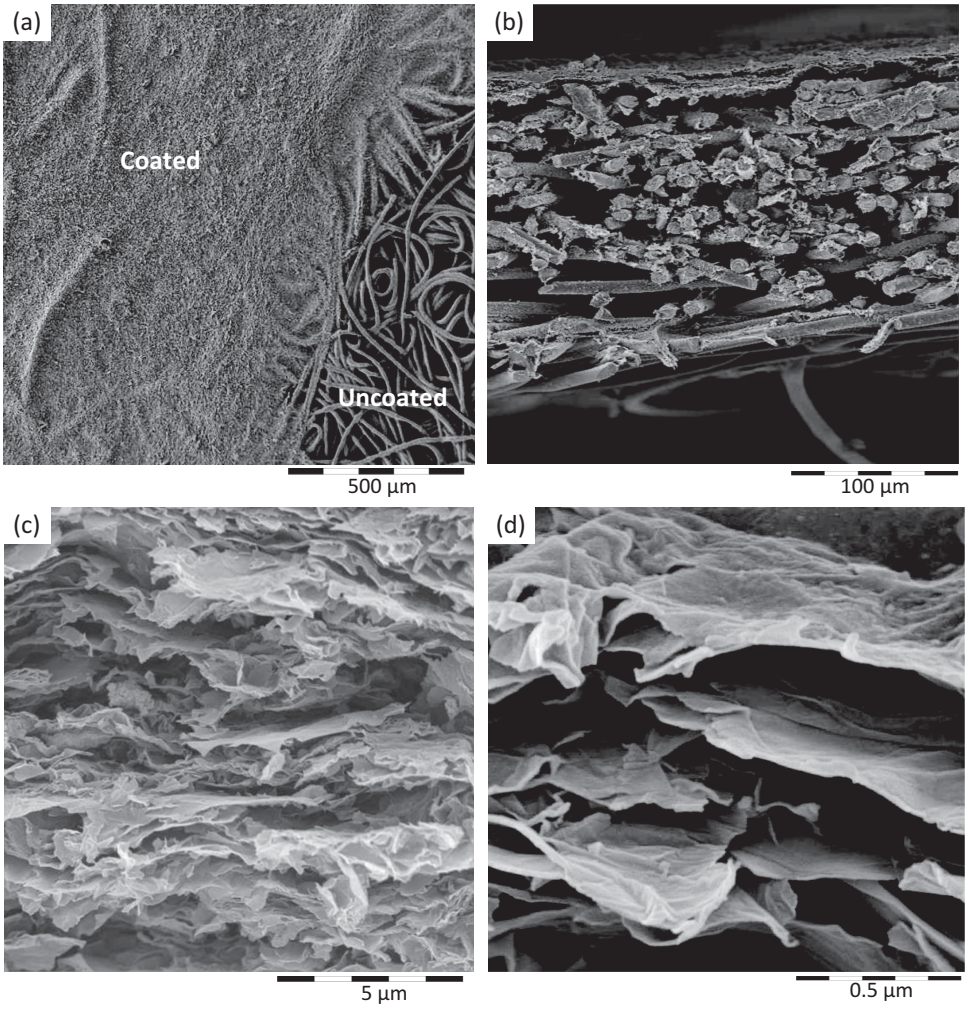

Figure 4. a) SEM image of TRGO printed on carbon cloth, b–d) cross-sectional observation of TRGO printed on carbon cloth.

electrolytes showed typical double layer capacitive behavior. The rectangular shape of the CVs was well preserved at almost all scan rates, while showing a linear increase in current density. Unlike activated carbon, the excellent CV shapes at such a high scan rate (15 V s^{-1}) demonstrate a very rapid current response during the anodic and cathodic potential sweep and fast diffusion of electrolyte at the electrode surface.[52,53]

TRGO electrodes in both the electrolyte behave in a similar fashion at all scan rates which is indicative of excellent rate performance. The gravimetric specific capacitances calculated at 5 mV s^{-1} for TRGO-KOH and TRGO-$TEABF_4$-ACN were 60 F g^{-1} and 12 F g^{-1}, respectively. As for the volumetric specific capacitances, the devices showed a value of 10 F cm^{-3} for TRGO-KOH and 8.5 F cm^{-3} for TRGO-$TEABF_4$-ACN. Volumetric specific capacitances for graphene based materials generally will show lower value as the TRGO powder used is of a very low bulk density (8×10^{-3} g cm^{-3}). The volumetric capacitance decreases to 4 F cm^{-3} and 3.5 F cm^{-3} for both aqueous and organic electrolyte respectively as the scan rate increases to 15 V s^{-1}, retaining 50% of its capacitance. Figure 4e shows pure capacitive behavior even at a high frequency range (inset). Unlike activated carbon, the absence of a porous electrode behavior for TRGO in KOH is quite evident by the absence of the semi-circle profile at high frequency regions which is in corroboration with the nitrogen adsorption/desorption data discussed above.[11] Although, a very small and incomplete semi-circle can be seen for TRGO in $TEABF_4$-ACN which could be attributed to the lower conductivity of the organic electrolyte. The ESR taken at the intercept point of the X-axis for TRGO in KOH and $TEABF_4$-ACN is 0.2 Ω and 0.6 Ω respectively which is higher than the electrochemically reduced graphene oxide (ERGO) material reported by Sheng et al.[13] This might be the reason for better performance of ERGO for AC line filtering application at high scan rate up to 400 V s^{-1}.[13]

The ultra-high rate charge and discharge characteristics of the ECs fabricated with TRGO are further confirmed using the Bode plot in Figure 4f. It compares the results with a conventional activated carbon based EC. The relaxation time constant, τ_o, which is taken at an ≈45° angle, where the real and the imaginary component have equal magnitude, is calculated using Equation 1 below, where f_o is the frequency at an –45° angle,[13]

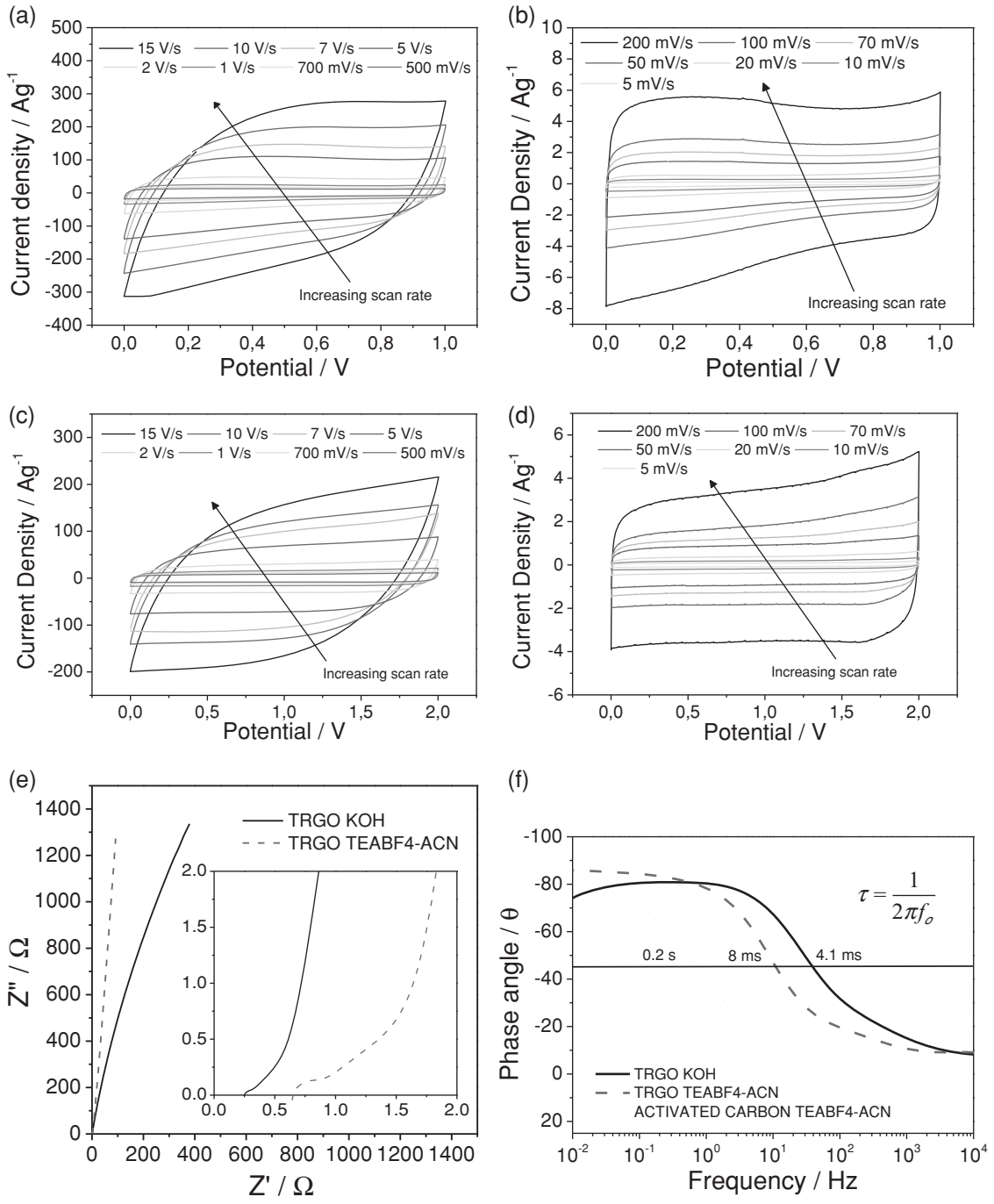

Figure 5. Cyclic voltammograms at different low and high voltage scanning rate in a,b) 1 M KOH. c,d) 1 M $TEABF_4$-ACN. e) Nyquist plot with inset of an expanded view in the high frequency region for TRGO in both $TEABF_4$-ACN and KOH. f) Impedance phase angle versus frequency plot; comparing TRGO-$TEABF_4$-ACN and TRGO-KOH with reference AC-EC.

$$\tau_o = \frac{1}{2\pi f_o} \quad (1)$$

τ_o for TRGO in KOH is 4.1 ms and TRGO in $TEABF_4$-ACN is 14.5 ms. The time constant value is smaller for KOH because of the fast adsorption and diffusion of K^+ ions on the electrode surface.

As highlighted earlier, slower ion adsorption in $TEABF_4$-ACN electrolyte is because of its high viscosity and large ion size which limits the ionic mobility across the electrolyte/electrode interface. Nevertheless, these results show that the ECs fabricated with TRGO demonstrated at least 10 times better frequency response than activated carbon (τ_o = 200 ms) in

Table 2. Time constant and capacitance values for TRGO in KOH and $TEABF_4$-ACN electrolytes.

Device IDs	Relaxation Time Constant at (–45° phase angle) [ms]	Time Constant at 100 Hz [ms]	Specific Capacitance at 100 Hz, C_{100Hz} [mF cm^{-2}]	Time Constant at 120 Hz [ms]	Specific Capacitance at 120 Hz, C_{120Hz} [mF cm^{-2}]
TRGO-KOH	4.1	2.5	3.88	2.3	3.55
TRGO-$TEABF_4$-ACN	14.5	4.4	1.96	3.8	1.76
Activated Carbon- $TEABF_4$-ACN	200	18.97	2.95	15.9	2.52

$TEABF_4$-ACN electrolyte. The RC time constants for TRGO is calculated by

$$\tau_{\text{frequency}} = RC = Z'\left(\frac{1}{2\pi f Z''}\right) \quad (2)$$

Where Z' is the resistive element, Z'' is the capacitive element and f is the frequency corresponding to it.

The RC time constants at 100 Hz and 120 Hz for TRGO in KOH were 2.5 ms and 2.3 ms respectively and for TRGO in $TEABF_4$-ACN were 4.4 ms and 3.8 ms respectively. The specific capacitance corresponding to the frequencies are so far the highest reported for graphene based ECs in both aqueous and organic medium.[11–13] All the above results are summarized in **Table 2**.

An ideal capacitor has a –90° phase angle shift between voltage and current at all frequencies. When the current is zero, voltage is at maximum, and vice versa. The instantaneous current flow is a measure of charges moving at that instant. When the system is fully charged, current will not be able to flow any further and the voltage will be at maximum. Subsequently, when the system is discharged, it drains the voltage to zero while drawing current at its maximum. Hence, the ratio between voltage and current is varying rapidly between zero and infinity.

The instantaneous voltage, V is

$$V = V_{\max} \sin \omega t \quad (3)$$

The instantaneous current, I is

$$I = I_{\max} \sin\left(\omega t + 90^{\circ}\right) \quad (4)$$

The lag between voltage and current is represented by

$$\theta = \tan^{-1}\left(\frac{X_c}{R}\right) \quad (5)$$

where R is the resistive element, X_c is the capacitive element and θ is the phase angle.

According to Equation 5, the ratio of X_c/R is undefined or does not exist (infinity) for an ideal capacitor where $R = 0$, as it consists only of the capacitive element X_c and the resistive element R. Hence, ideally the phase angle here will be –90°. However, in practical applications, this value is not possible because of the presence of resistance in the system. Since the ratio between X_c (Z'') and R (Z') determines the phase angle,[54] the co-existence of these two variables makes the evaluation of the pure capacitive behavior, by phase angle alone, challenging. Many have reported the "factor of merit" in the literature indicating a high phase angle close to –90° at 120 Hz as the evaluating parameter for high capacitance devices.[11,13] It is somewhat misleading and may not be accurate for all cases. In here, the specific capacitance reported at 100/120 Hz is in fact higher than those reported in the literature but the phase angle is not closer to –90°. This contradicts the justifications given in the literature. The contribution of resistance influences the X_c/R ratio and gives a phase angle lesser than –90°. The phase angles recorded for TRGO in both aqueous and organic electrolyte were around –30° at 120 Hz. This value is still higher than that of porous activated carbon which normally will result in near 0° at 120 Hz.[11] As observed in the nitrogen adsorption and desorption isotherm, the pore structure of the TRGO is not the same as for activated carbon. AC signal propagation varies according to geometry of pores, especially when two types of pore geometry co-exist.[55] In our case, TRGO of slit pore type is printed on carbon cloth which is fibrous. This could be one of the contributing factors for the occurrence of lower phase angle than reported by others.[11,13]

Miller et al. reported that the transition between the inductive and capacitive behavior, which takes place from high to low frequency at near –90° phase angle for graphene based ECs, occurs over a single decade, while for activated carbon it has been seen over seven decades of frequencies.[11] Similarly, our system confirms this occurrence where TRGO takes approximately one to three decades of frequency for the transition. The reason for the variation of our results compared to the earlier work is because of the fact that TRGO has structural defects that limits fast electron mobility. This limitation causes the prolonged transition between the inductive and capacitive behavior.

From the galvanostatic charge-discharge (CD) profile shown in **Figure 6**a–d, a linear CD behavior with constant slope can be observed which reveals nearly ideal EC characteristics involving efficient ion transport across the electrodes. These ECs are able to be rapidly (re)charged and discharged on a very short time scale down to milliseconds. The ESR values calculated from IR drop during discharge agree with values taken from the impedance analysis.

At a slow discharge rate of 1.25 A g^{-1} TRGO in KOH exhibits 0.46 Ω. It increases to 0.73 Ω as the discharge current density increases to 125 A g^{-1}. The energy and power densities were determined using

$$E = \frac{1}{2}V^2\left[\text{Wh kg}^{-1}\right] \quad (6)$$

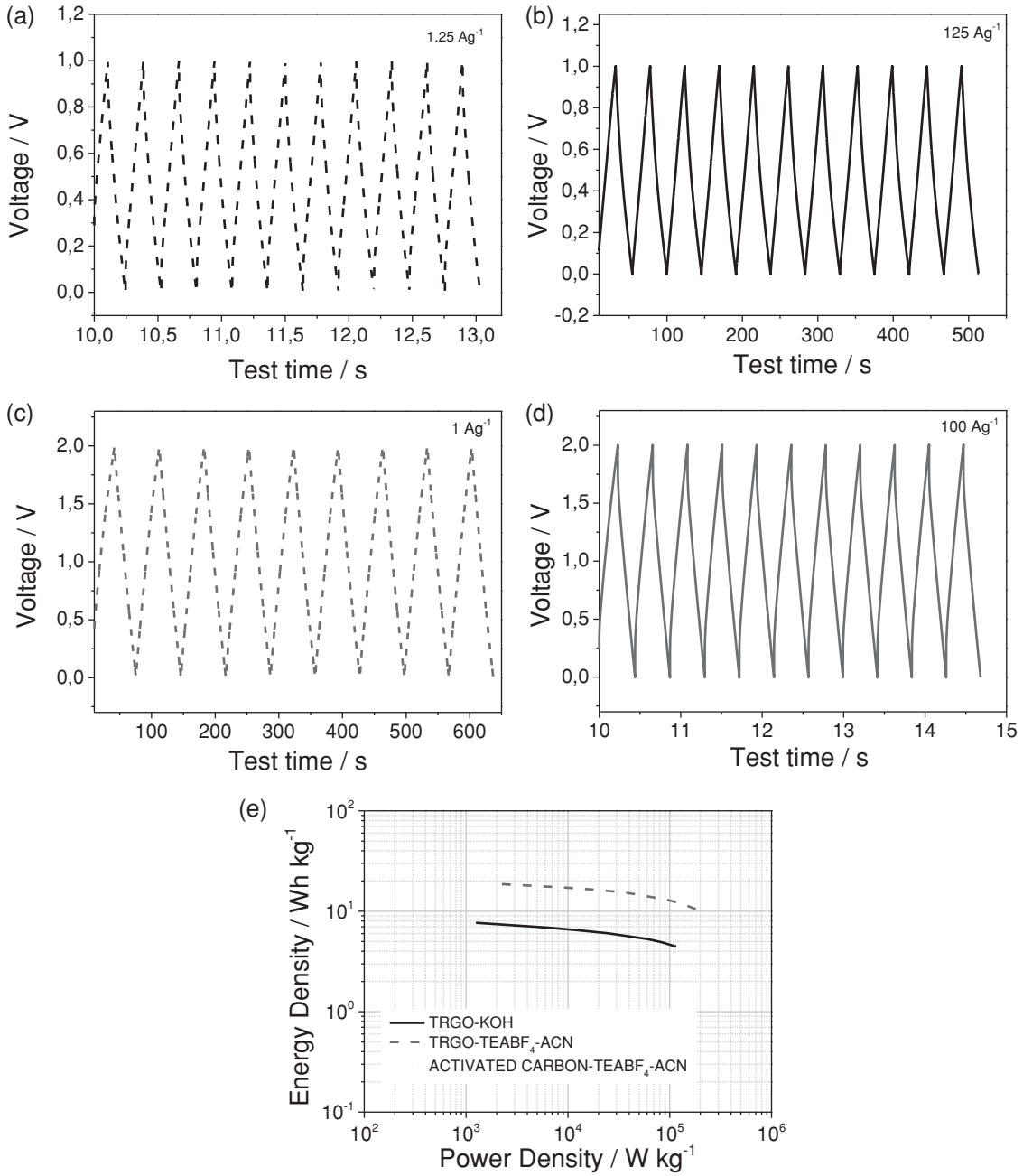

Figure 6. Charge/Discharge curve for TRGO in KOH at a) 1.25 A g^{-1}. b) 125 A g^{-1}.; TRGO in $TEABF_4$-ACN. c) 1.00 A g^{-1} d) 100 A g^{-1}. e) Power and energy density comparison at various constant currents for TRGO-KOH and TRGO-$TEABF_4$-ACN.

$$P = \frac{E}{t}\left[\mathrm{W\ kg^{-1}}\right] \quad (7)$$

As shown in the Ragone plot in Figure 5e, TRGO in $TEABF_4$-ACN (4.43 mWh cm^{-3}) obviously showed better energy density than TRGO in KOH (1.46 mWh cm^{-3}) because of the high working potential which is 2 V. TRGO in $TEABF_4$-ACN also demonstrated impressive power capability up to 42.74 kW cm^{-3}. These results are much superior (at least one order of magnitude higher) than the values reported in the literature for high energy devices using graphene based materials.[9,10,56] **Table 3** summarizes the power and energy density of both the ECs.

3. Conclusion

We developed a novel process using 3D micro-extrusion for the fabrication of binder and surfactant free functionalized graphene based electrodes that are of high charge/discharge capability. Highly concentrated and conductive graphene

Table 3. Configurations of the fabricated ECs devices and electrochemical testing results.

Device IDs	Energy density [Wh kg^{-1}][a)]	Power density [kW kg^{-1}][b)]	Energy density [mWh cm^{-3}][a)]	Power density [kW cm^{-3}][b)]
TRGO-KOH	7.68	115.80	1.46	21.95
TRGO-TEABF$_4$-ACN	18.72	180.40	4.43	42.74
Laser Scribed Graphene[9]	/	/	1.36	0.020
GO film reduced by methane (CH_4)–plasma treatment graphene-based in-plane micro SC[10]	/	/	2.5	0.495
Laser Scribed Graphene micro SC[53]	/	/	~1	0.200

[a)]Calculated from constant current technique; [b)]Measured after the voltage drop. *All calculations were made using the mass of the active materials.

dispersions containing up to 15 g L^{-1} of single and few layered TRGO sheets were produced by the high pressure homogenization (HPH) method. High SSA of 593 m^2 g^{-1} and good conductivities up to 16 S cm^{-1} were measured from the TRGO material. Based on the process of controlled 3D-micro-extrusion of the TRGO dispersions, functionalized graphene-based active electrodes of high SSA and conductivities were fabricated on carbon substrates. ECs constructed with these TRGO electrodes demonstrated volumetric capacitances of 10 F cm^{-3} in 1 M KOH and 8.5 F cm^{-3} in 1 M TEABF$_4$-ACN. They also have impressive charge storage performances that can be charged and discharged at a very high rate with a RC time constant at 120 Hz of 2.3 ms and 3.8 ms in both aqueous and non-aqueous electrolyte, respectively. The capacitance values derived at 120 Hz were 3.55 mF cm^{-2} and 1.76 mF cm^{-2} for both, the aqueous and non-aqueous system. TRGO-TEABF$_4$-ACN showed an energy density of 4.43 mWh cm^{-3} and also demonstrated impressive power capability up to 42.74 kW cm^{-3}. The 3D microextrusion printing process for printable functionalized graphene is clearly a very versatile electrode fabrication technique that could lead to a new class of entirely printable charge storage devices for ac-line filtering. Graphene based ECs have great potential in replacing electrolytic capacitors as they provide better performances in terms of frequency response, low ESR, high specific capacitance and high power and energy density.

4. Experimental Section

Preparation of GO and TRGO: Preparations of GO and TRGO were carried through as described earlier.[14] The reduction temperature of 400°C was applied during the thermal exfoliation and reduction in the tube furnace.

Physical Characterizations of Materials: Atomic force microscope (AFM) analysis were conducted using a Nanoscope III scanning probe-microscope (Veeco). Transmission electron microscope (TEM) images were taken using a LEO 912 Ω (Zeiss) with an acceleration voltage of 120 kV. Nitrogen adsorption and desorption measurements were performed at liquid nitrogen temperature using a ASAP 2420 system (Micromeritics). The samples were degassed and dried for 5 h at 150 °C prior to the measurement. Surface areas were determined using the Brunauer, Emmett and Teller (BET) method. The morphology of the samples was analyzed with a field emission scanning electron microscope (FE-SEM) Gemini Ultra 55 (Zeiss). Raman spectra were recorded with a NT-DMT Ntergra Spectra system using laser excitation at 514 nm. The electrical conductivity was measured using a Keithley Elektrometer 617 with a four-point-probe arrangement.

Preparation of Highly Concentrated TRGO Dispersion: Highly concentrated TRGO dispersions in *iso*-propanol (15 g L^{-1}) were produced by modified laboratory high-pressure-homogenizer (NS1001L Panda 2K, GEA Niro Soavi, Germany) using a pressure of 1000 bar.

Fabrication of Graphene-based Electrode by 3D Microextrusion: The prepared dispersions were processed by the low-temperature print head of the 3D Bioplotter (3rd generation, Envisiontec, Gladbeck, Germany). Circles of an inner diameter of 16 mm and a thickness of about 21 µm were printed onto carbon fabrics (H2315 IX 11, Freudenberg). The mass of each film was determined by the weight difference before and after printing. This value is taken for volumetric capacitance which includes the weight and the thickness of the substrate.

Fabrication of Activated Carbon-based Electrode: A slurry comprising 80% of activated carbon (DARCO KB-G, Norit), 10% of additive carbon (Super P, Timcal) and 10% carboxymethylcellulose (CMC, Sigma Aldrich) was prepared using *iso*-propanol and distilled water. The slurry was then coated onto aluminium foil using doctor blade into a thin film of uniform thickness (180 µm) and dried in a vacuum oven at 60 °C for 24 h. Circular disks of 16 mm diameter were punched out for EC fabrication. This EC is used as comparison for impedance analysis and nitrogen adsorption and desorption measurements against TRGO.

Assembly and Electrochemical Characterizations of ECs: Symmetric two-electrodes ECs were assembled in a stainless steel EC cell with titanium electrodes using TRGO printed on the carbon fabric substrate (diameter 16 mm). All electrochemical measurements were carried out using 1 M of potassium hydroxide (KOH) in water or 1 M of tetraethyl ammonium tetrafluoroborate in acetonitrile (TEABF$_4$-ACN) as the electrolyte. Activated carbon based ECs were assembled in a similar fashion using 1 M of tetraethyl ammonium tetrafluoroborate in acetonitrile (TEABF$_4$-ACN) as the electrolyte. The electrochemical impedance spectroscopy, cyclic voltammetry, and galvanostatic charge-discharge were measured using an electrochemical workstation Biologic Potentiostat/Galvanostat MPG2 and Gamry MultiEchem Potentiostat/Galvanostat/ZRA system at room temperature.

Acknowledgements

The authors would like thank Dr. Digvijay Thakur (BASF SE) for his help in Raman spectra analysis. T.N.-W. and I.-M.L. contributed equally to this work.

Received: December 12, 2013
Revised: February 6, 2014
Published online: May 2, 2014

[1] A. Nishino, *J. Power Sources* **1996**, *60*, 137.
[2] K.-L. Wang, R.-F. Chang, *J. Power Sources* **2006**, *162*, 1455.
[3] S. S. Park, B. T. Lee, *J. Electroceram.* **2004**, *13*, 111.
[4] J. R. Miller, P. Simon, *Science* **2008**, *321*, 651.

[5] P. Simon, Y. Gogotsi, *Nat. Mater.* **2008**, *7*, 845.
[6] M. Rosa Palacin, *Chem. Soc. Rev.* **2009**, *38*, 2565.
[7] C. Liu, Z. Yu, D. Neff, A. Zhamu, B. Z. Jang, *Nano Lett.* **2010**, *10*, 4863.
[8] L. Dai, *Acc. Chem. Res.* **2013**, *46*, 31.
[9] M. F. El-Kady, R. B. Kaner, *Nat. Commun.* **2013**, 4.
[10] Z.-S. Wu, K. Parvez, X. Feng, K. Muellen, *Nat. Commun.* **2013**, 4.
[11] J. R. Miller, R. A. Outlaw, B. C. Holloway, *Science* **2010**, *329*, 1637.
[12] P. Kossyrev, *J. Power Sources* **2012**, *201*, 347.
[13] K. Sheng, Y. Sun, C. Li, W. Yuan, G. Shi, *Scientific Reports* **2012**, 2.
[14] F. J. Toelle, M. Fabritius, R. Muelhaupt, *Adv. Funct. Mater.* **2012**, *22*, 1136.
[15] L. T. Le, M. H. Ervin, H. Qiu, B. E. Fuchs, W. Y. Lee, *Electrochem. Commun.* **2011**, *13*, 355.
[16] J. Li, F. Ye, S. Vaziri, M. Muhammed, M. C. Lemme, M. Ostling, *Adv. Mater.* **2013**, *25*, 3985.
[17] Y. Xu, I. Hennig, D. Freyberg, A. J. Strudwick, M. G. Schwab, T. Weitz, K. C. Cha, *J. Power Sources* **2014**, *248*, 483.
[18] Y. Xu, M. G. Schwab, A. J. Strudwick, I. Hennig, X. Feng, Z. Wu, K. Müllen, *Adv. Energy Mater.* **2013**, *3*, 1035.
[19] B. J. de Gans, P. C. Duineveld, U. S. Schubert, *Adv. Mater.* **2004**, *16*, 203.
[20] V. Dua, S. P. Surwade, S. Ammu, S. R. Agnihotra, S. Jain, K. E. Roberts, S. Park, R. S. Ruoff, S. K. Manohar, *Angew. Chem. Int. Ed.* **2010**, *49*, 2154.
[21] M. Lotya, P. J. King, U. Khan, S. De, J. N. Coleman, *Acs Nano* **2010**, *4*, 3155.
[22] E. B. Secor, P. L. Prabhumirashi, K. Puntambekar, M. L. Geier, M. C. Hersam, *J. Phys. Chem. Lett.* **2013**, *4*, 1347.
[23] C. Wang, D. Li, C. O. Too, G. G. Wallace, *Chem. Mater.* **2009**, *21*, 2604.
[24] http://www.nanointegris.com/en/puresheets (accessed January 2014).
[25] Y. Hernandez, V. Nicolosi, M. Lotya, F. M. Blighe, Z. Sun, S. De, I. T. McGovern, B. Holland, M. Byrne, Y. K. Gun'ko, J. J. Boland, P. Niraj, G. Duesberg, S. Krishnamurthy, R. Goodhue, J. Hutchison, V. Scardaci, A. C. Ferrari, J. N. Coleman, *Nat. Nanotechnol.* **2008**, *3*, 563.
[26] T. Hasan, F. Torrisi, Z. Sun, D. Popa, V. Nicolosi, G. Privitera, F. Bonaccorso, A. C. Ferrari, *Phys. Status Solidi B* **2010**, *247*, 2953.
[27] R. Landers, R. Mülhaupt, *Macromol. Mater. Eng.* **2000**, *282*, 17.
[28] R. Landers, A. Pfister, U. Hubner, H. John, R. Schmelzeisen, R. Mulhaupt, *J. Mater. Sci.* **2002**, *37*, 3107.
[29] H. C. Schniepp, J. L. Li, M. J. McAllister, H. Sai, M. Herrera-Alonso, D. H. Adamson, R. K. Prud'homme, R. Car, D. A. Saville, I. A. Aksay, *J. Phys. Chem. B* **2006**, *110*, 8535.
[30] M. J. McAllister, J.-L. Li, D. H. Adamson, H. C. Schniepp, A. A. Abdala, J. Liu, M. Herrera-Alonso, D. L. Milius, R. Car, R. K. Prud'homme, I. A. Aksay, *Chem. Mater.* **2007**, *19*, 4396.
[31] H. L. Poh, F. Sanek, A. Ambrosi, G. Zhao, Z. Sofer, M. Pumera, *Nanoscale* **2012**, *4*, 3515.
[32] K. S. Novoselov, V. I. Falko, L. Colombo, P. R. Gellert, M. G. Schwab, K. Kim, *Nature* **2012**, *490*, 192.
[33] D. R. Dreyer, S. Park, C. W. Bielawski, R. S. Ruoff, *Chem. Soc. Rev* **2009**, *39*, 228.
[34] H. L. Poh, F. Šaněk, A. Ambrosi, G. Zhao, Z. Sofer, M. Pumera, *Nanoscale* **2012**, *4*, 3515.
[35] S. J. Gregg, K. S. W. Sing, *Adsorption, Surface Area and Porosity*, Academic Press, London **1982**.
[36] K. S. W. Sing, D. H. Everet, R. A. W. Haul, L. Moscou, R. A. Pierotti, J. Rouquerol, T. Siemeniewska, *Pure Appl. Chem.* **1985**, *57*, 603.
[37] Y. Huang, J. Liang, Y. Chen, *Small* **2012**, *8*, 1805.
[38] H. Jiang, P. S. Lee, C. Li, *Energy Environ. Sci.* **2013**, *6*, 41.
[39] A. C. Ferrari, J. C. Meyer, V. Scardaci, C. Casiraghi, M. Lazzeri, F. Mauri, S. Piscanec, D. Jiang, K. S. Novoselov, S. Roth, A. K. Geim, *Phys. Rev. Lett.* **2006**, 97.
[40] C. N. R. Rao, A. K. Sood, K. S. Subrahmanyam, A. Govindaraj, *Angew. Chem. Int. Ed.* **2009**, *48*, 7752.
[41] A. K. Geim, K. S. Novoselov, *Nat. Mater.* **2007**, *6*, 183.
[42] Q. Liu, Z. Liu, X. Zhang, L. Yang, N. Zhang, G. Pzn, S. Yin, Y. Chen, J. Wei, *Adv. Funct. Mater.* **2009**, *19*, 894.
[43] M. D. Stoller, S. Park, Y. Zhu, J. An, R. S. Ruoff, *Nano Lett.* **2008**, *8*, 3498.
[44] B. Fang, L. Binder, *Electrochim. Acta* **2007**, *52*, 6916.
[45] H. Oda, A. Yamashita, S. Minoura, M. Okamoto, T. Morimoto, *J. Power Sources* **2006**, *158*, 1510.
[46] U. Khan, A. O'Neill, M. Lotya, S. De, J. N. Coleman, *Small* **2010**, *6*, 864.
[47] Y. T. Liang, M. C. Hersam, *J. Am. Chem. Soc.* **2010**, *132*, 17661.
[48] F. Torrisi, T. Hasan, W. Wu, Z. Sun, A. Lombardo, T. S. Kulmala, G.-W. Hsieh, S. Jung, F. Bonaccorso, P. J. Paul, D. Chu, A. C. Ferrari, *ACS Nano* **2012**, *6*, 2992.
[49] http://www.microdrop.de (accessed November 2013).
[50] Y. Wang, Z. Shi, Y. Huang, Y. Ma, C. Wang, M. Chen, Y. Chen, *J. Phys. Chem. C* **2009**, *113*, 13103.
[51] N. Jha, P. Ramesh, E. Bekyarova, M. E. Itkis, R. C. Haddon, *Adv. Energy Mater.* **2012**, *2*, 438.
[52] W. Gao, N. Singh, L. Song, Z. Liu, A. L. M. Reddy, L. Ci, R. Vajtai, Q. Zhang, B. Wei, P. M. Ajayan, *Nat. Nanotechnol.* **2011**, *6*, 496.
[53] P. Chen, J.-J. Yang, S.-S. Li, Z. Wang, T.-Y. Xiao, Y.-H. Qian, S.-H. Yu, *Nano Energy* **2013**, *2*, 249.
[54] A. Lasia, in *Modern Aspects of Electrochemistry*, Vol. *32* (Eds: B. E. Conway, R. E. White, J. O. M. Bockris), Kluwer Academic/Plenum Publishers, New York **1999**, 143.
[55] M. M. E. Duarte, M. M. Stefenel, C. E. Mayer, *J. Argent. Chem. Soc.* **2002**, *90*, 111.
[56] M. F. El-Kady, V. Strong, S. Dubin, R. B. Kaner, *Science* **2012**, *335*, 1326.